CrossMark

ORIGINAL PAPER

Chromia Scale Thermally Grown on Pure Chromium Under Controlled $p(O_2)$ Atmosphere: I. Spallation Investigation Using Photoelectrochemical Techniques at a Mesoscale

L. Latu-Romain[1] · Y. Parsa[1] · S. Mathieu[2] · M. Vilasi[2] · Y. Wouters[1] (iD)

Abstract Chromia scales isothermally grown on pure chromium at 900 °C and a $p(O_2)$ of 10^{-12} atm during 30 min exhibit n- and p-type conduction associated with a duplex morphology with an internal equiaxed subscale for an inward (anionic) growth and an external columnar subscale for an outward (cationic) growth. After oxidation exposure, spalled regions in the oxide scale can be observed and have been studied with photoelectrochemical techniques at a mesoscale (probe diameter in the range of 50 μm). Owing to the semiconducting properties of each subscale (bandgap and conduction type), a scenario of spallation is proposed and clarifies when and where the oxide scale spallation occurs.

Keywords Chromia · Photoelectrochemistry · TEM characterization · Spallation

Introduction

Chromia-forming alloys are well known to be widely used in aggressive environments (high temperature, oxidizing atmosphere) because of their ability to form a protective layer. If numerous studies have been conducted on these alloys during the last decades, most of the works related to pure chromium oxidation and pure chromia scales properties have been published during the 1970s, 1980s and 1990s [1–12] and refer, most of the time, to electrical conductivity, tracers experiments and isotopic tracers studies. Kofstad, in his well-known book "High temperature corrosion" published in 1988 [13], writes about non stoichiometry of

✉ Y. Wouters
yves.wouters@univ-grenoble-alpes.fr

1   SIMaP, CNRS, Université Grenoble Alpes, 38000 Grenoble, France

2   IJL, Université de Lorraine, 54011 Nancy, France

chromia that: "It does not appear possible to draw any definitive conclusions about defect structure of Cr_2O_3 from these measurements." Of course, he is talking about a review of different works at the beginning of a chapter devoted to chromia. Later in the book, he adds: "Additional studies are necessary in this oxide in order to obtain a detailed understanding of its defect structure and transport properties." Twenty years later, Young, in his well-known book "High temperature oxidation and corrosion of metals" published in 2008 [14], concerning chromia, writes: "The oxygen potential effects are not well understood…." Nowadays, we have no choice but to note that the present situation remains not clear. However, several main lines can be extracted. First, chromia is a dual semiconductor, sometimes *n*-type sometimes *p*-type. The ionic disorder changes with temperature and oxygen activity. Secondly, outward chromium and inward oxygen diffusion have been reported in several studies depending on temperature and oxygen partial pressure. Thirdly, the grain boundaries play an important role; lattice diffusion has been measured in single crystal Cr_2O_3 and found to be extremely slow [9, 11, 12]. Fourthly, several studies report a duplex morphology with equiaxed, basaltic or columnar grains, depending on the oxidation conditions [6, 15]. Finally, many works report that the oxidation kinetic follows a parabolic law.

Recent works in our research group [16–20] have shown that whatever $p(O_2)$ may be, chromia scales grown on pure chromium in the range 800–900 °C reveal a duplex morphology with an internal equiaxed subscale growing inwards and an external columnar subscale growing outwards. The internal subscale always exhibits *n*-type conduction, while the external subscale shifts from *n*-type to insulator and finally to *p*-type conduction when $p(O_2)$ is increased (from 10^{-14} to 10^{-12} atm).

The present paper is focused on spallation which can be sometimes observed on samples oxidized at 900 °C and $p(O_2) \sim 10^{-12}$ atm. In order to elucidate when and where this phenomenon occurs, the semiconducting signature of each subscale (bandgap and conduction type) has been investigated with photoelectrochemical techniques at a mesoscale, i.e., with a probe diameter in the range of 50 μm.

Experimental Procedures

Pure chromium (99.99% purity, from Goodfellow SARL, France) was oxidized at 900 °C and a $p(O_2) \sim 10^{-12}$ atm during 30 min. Before oxidation, Cr samples were cut from a plate to the dimension $10 \times 10 \times 1$ mm and were SiC ground up to the grade 320. Oxidation tests had been carried out with the Rhines pack method [21]. The sample is placed on an alumina crucible (see Fig. 1). This crucible is itself positioned in a silica tube containing nickel/bunsenite buffering powder mixture which ensures the control of the oxygen activity during the oxidation step. Before being sealed, the tube is connected to a vacuum station. Once the pressure value falls below 10^{-6} atm, the tube is filled with Ar (99.9999% in purity) in order to reach a total pressure in the tube of 1 atm at the oxidation temperature. Finally, the sealed tube is placed in a furnace at 900 °C for 30 min and then cooled in air. Many buffers can be used in the Rhines pack: magnetite/hematite, iron/wüstite, nickel/bunsenite, etc. But buffers containing iron are problematic because iron is able to
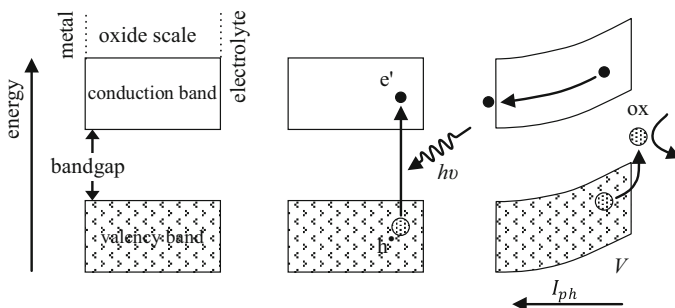
Fig. 1 Schematic representation of the Rhines pack reactor

T = 900 °C
$P(O_2) \sim 10^{-12}$ atm
$P(Ar) \sim 1$ atm

sealed tube

sample

alumina crucible

Ni/NiO powder
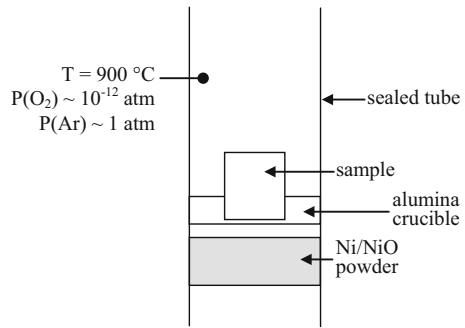
diffuse through the atmosphere to the sample and to dramatically change the properties of chromia [22]. Consequently, nickel/bunsenite buffering powder mixture was chosen in this work. At 900 °C, the calculated oxygen partial pressure $p(O_2)$ imposed by this buffer is equal to 10^{-12} atm. This value has been obtained with Factsage 7.0TM software using a coherent set of pure substances from the FACT pure substances database 2012 [22].

In these conditions, oxide scale thickness has been estimated in the micrometer range, the value required to perform adequate photoelectrochemical analysis.

Photoelectrochemistry (PEC) is an ex situ nondestructive method which uses the photon as a probe and has been extensively described elsewhere [16]. After oxidation and cooling, the oxide scale is used as the working electrode (area exposed to the electrolyte is ~ 0.2 cm^2) in a classical three-electrode electrochemical cell and behaves like a semiconductor (see Fig. 2). A monochromatic light can induce the photogeneration of electron–hole pairs as soon as the provided energy $E = h\upsilon$ is higher than the bandgap E_g. Then, the collection of these electron–hole pairs becomes possible when an electrochemical potential V is applied to the system. Due to the band bending, the hole $h^{\cdot}$ is transmitted to an appropriate redox species in the electrolyte and the electron e' is collected through the scale to the internal interface (for a n-type semiconductor). The sum of these steps leads to the production of a current so-called photocurrent I_{ph}. When the photocurrent is measured as a function of the energy of the incident light, the bandgap energy can


Fig. 2 Schematic representation of the photocurrent generation

be extracted, whereas the study of the evolution of photocurrent as a function of the applied potential permits to determine the conduction type. All the experiments in this work were carried out at room temperature in an aqueous solution of sodium sulfate (0.1 mol L^{-1}, pH = 8), using a platinum foil (area $\sim$ 1 cm^2) as the counter electrode and a mercury–mercurous sulfate electrode (MSE) as the reference electrode (+ 0.650 V vs. standard hydrogen electrode).

To allow experiments at the mesoscopic scale, the light of a xenon arc light source (Newport, model 6255) was focused on a spot of about 50 μm diameter. The focus was obtained using achromatic aluminum mirrors which offered a wide range of working distances. This localized analysis is so-called mesoPEC in the rest of this paper.

Results and Discussion

A previous work [16, 18] has shown that the oxide scale grown on pure chromium in the present conditions (900 °C, $p(O_2) \sim 10^{-12}$ atm, t = 30 min) was made of pure chromia with submicronic grains. DRX and Raman spectroscopy have confirmed the presence of a single-crystalline structure: the eskolaite (JCPDS card 38-1479) [18, 20, 22]. Sometimes, spalled zones can be observed on the samples. Figure 3a presents a classical example of a spalled zone of several hundred of square micrometers in area. All around this zone, the oxide scale appears debonded in a few micrometer bands in length. In the non-spalled region, the STEM bright-field cross-sectional view (Fig. 3b) shows a duplex morphology with a columnar external subscale and an equiaxed internal subscale (total thickness in the range of 1.5 μm). On this figure, several grain boundaries have been underlined and one can observe a very clear limit between these two subscales. It should be also noted that some voids of a few hundreds of nanometers in diameter can be observed in the internal subscale more or less localized at the metal/oxide interface (in white). Figure 3c presents an SEM fractography in the spalled zone and clearly shows the presence of a thin and covering oxide scale of about 200 nm in thickness.
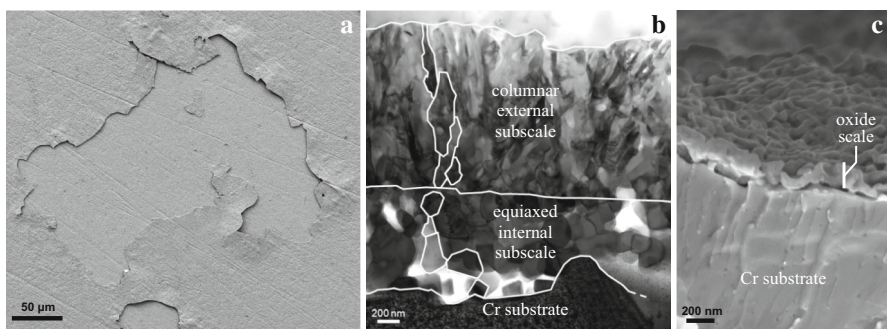

Fig. 3 Chromia scale thermally grown at 900 °C and a $p(O_2) \sim 10^{-12}$ atm during 30 min, **a** SEM top-view (SE detector), **b** bright-field cross-sectional view STEM in the non-spalled region, **c** SEM fractography (InLens detector, tilt $\sim$ 30°) in the spalled region
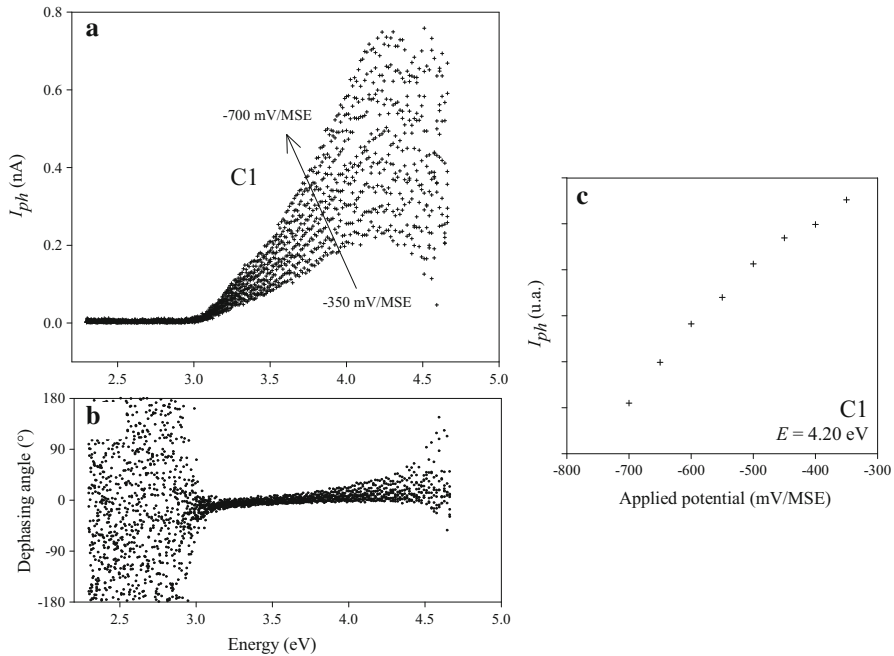
The mesoPEC analysis of the non-spalled region is presented in Fig. 4. The energy spectra (Fig. 4a) obtained at different applied potentials exhibit two photocurrent contributions ($C1$ and $C2$) with an inversion of the photocurrent sign as evidenced by the dephasing angle evolution of about 180° (Fig. 4b). Typically, this inversion is due to a change of conduction from one contribution to another. Classical transforms described elsewhere [23] ($I_{\mathrm{ph}} E^{1/n} = f(E)$, not presented here) lead to the determination of 2 bandgaps: $E_g \sim 3.0$ eV for $C1$ and $E_g \sim 3.6$ eV for $C2$. By extracting the photocurrent of $C1$ and $C2$ at a given energy, here at 3.15 eV for $C1$ (Fig. 4c) and at 4.75 eV for $C2$ (Fig. 4d), it can be observed that $C1$ conduction is mainly n (the photocurrent increases with the applied potential), while $C2$ conduction is mainly p (the photocurrent decreases with the applied potential).

The mesoPEC analysis of the spalled region is presented in Fig. 5. Contrary to what could be observed on non-spalled region, the $C2$ contribution is no longer detected on the energy spectra and only one contribution can be recorded; the $C1$ contribution with a bandgap E_g around 3.0 eV. The presence of only one contribution is confirmed with the stability near 0° of the dephasing angle (Fig. 5b) in the whole range of energy. Figure 5c also confirms that $C1$ conduction remains mainly n (the photocurrent increases with the applied potential).

A previous work [16] has shown that the $C1$ (resp. $C2$) contribution can be associated with the internal (resp. external) subscale. The evidence of the depth
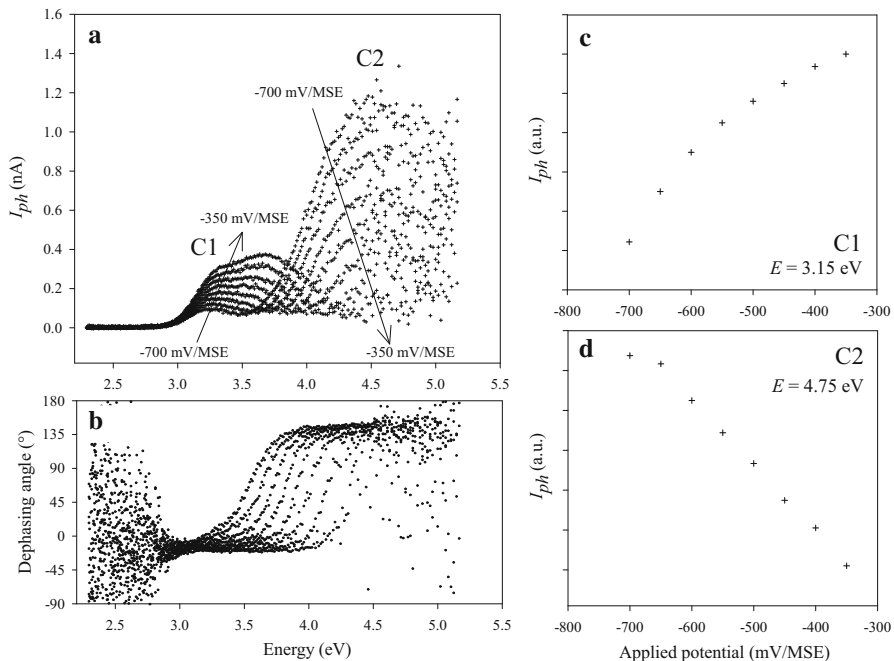
Fig. 4 MesoPEC analysis of the non-spalled region: **a** photocurrent (I_{ph}) and **b** dephasing angle versus incident light energy (E) recorded at several applied potentials (V) varying from − 700 to − 350 mV/ MSE, with a 50 mV step, **c, d** photocurrent versus applied potential (V) at 3.15 and 4.75 eV from − 700 to − 350 mV/MSE, with a 50 mV step

Fig. 5 MesoPEC analysis of the spalled region: **a** photocurrent (I_{ph}) and **b** dephasing angle versus incident light energy (E) recorded at several applied potentials (V) varying from -700 to -350 mV/MSE, with a 50 mV step, **c** photocurrent versus applied potential (V) at 4.20 eV from -700 to -350 mV/MSE, with a 50 mV step

distribution of C1 and C2 was in particular confirmed with PEC measurements after successive polishing treatment of the scale. Together with TEM ASTAR results, it was also possible to associate with each subscale a direction of growth and to clarify the nature of the major point defect. The results are summarized in Table 1. From these data, the Brouwer diagram of this system was drawn and a kinetic modeling consistent with all experimental observations has been proposed.

In the present work, spalled regions can be observed and two questions can arise. When and where occurs the separation of the scale? In oxide scales, the mechanical stress is well known to have mainly two origins. The first one occurs during isothermal growth and corresponds to the mismatch between the volume of the elementary cell of the chromia and the volume of the elementary cell of the corresponding metal. In the present system, the Pilling and Bedworth ratio (PBR) is

Table 1 Principal results obtained in previous works [16, 18–20]

Subscale	Morphology	PEC contribution	E_g (eV)	Conduction	Growth	Major point defects
Internal	Equiaxed	C1	~ 3.0	n	Inward	$V_O^{\cdot\cdot}$
External	Columnar	C2	~ 3.6	p	Outward	$V_{Cr}^{\prime\prime\prime}$

equal to the substantial value of 2.07 [24], but its effect remains under discussion in the literature. Indeed, the outward growth of the external subscale does not probably generate any stress, but the inward growth of the internal subscale may generate compressive stress. In addition, models incorporating the generation of new oxide at grain boundary inside the volume of the already existing scale may also generate large compressive stress during oxidation [25] and is probably able to generate cracks and buckling in the scale. The second source of stress occurs during cooling and is the result of very large differences between the thermal expansion coefficients of the oxide and the metal. α_{Cr} is reported $\sim 10^{-5}$ K^{-1} [26] when $\alpha_{Cr_2O_3}$ exhibits a value lying between 5.7 and 9.6 $\times 10^{-6}$ K^{-1} [26–34]. Consequently, the ratio $\alpha_{Cr}/\alpha_{Cr_2O_3}$ is generally accepted to be close to 1.3. Several works underline that chromia spallation often occurs during cooling [35, 36], and some others report a very high residual stress close to 2 GPa [37–39]. In addition, the presence of voids in the oxide scale, probably as a result of the diffusion mechanism, previously observed at the beginning of "Results and Discussion" section can represent an important factor of delamination. In conclusion, buckling of the oxide scale is able to take place at any interface during the isothermal oxidation, probably due to the PBR effect, but spallation possibly occurs during the sample cooling due to the large differences between the thermal expansion coefficients of the oxide and the metal. For example, detection of cracking or buckling has been recently detected with acoustic emission (AE) during pure chromium oxidation at 1050 °C in synthetic air but also during cooling [40].

In the first instance, we must observe that the spallation certainly occurs during the sample cooling. Indeed, if the spallation had occurred during the oxidation, two hypotheses would have to be considered:

- Firstly, the separation of the scale occurs at the metal/oxide interface and the metal is again oxidized with a duplex structure $C1$ (*n*-type) and $C2$ (*p*-type).
- Secondly, the separation of the scale occurs at the $C1/C2$ interface and the external part of $C1$, in contact with the oxidizing atmosphere, reaches the thermodynamic equilibrium. As a result, it shifts to a *p*-type conduction (i.e., $C2$).

In both hypotheses, the presence of a *p*-type semiconductor contribution ($C2$) is expected in the spalled region, but only $C1$ is detected in Fig. 5. These assumptions must therefore be rejected.

Consequently, we might consider that the spallation occurs during the cooling. A first scenario consists in the separation of the external subscale via a classical process of buckling as presented in Fig. 6. In this first scenario, it is assumed that the interface located in the oxide scale between the internal and the external subscale ($C1/C2$ interface) is the most fragile. This proposal would be in good agreement with the mesoPEC results, in particular the presence of *n*-type chromia detected in the spalled region.

To validate this first scenario, a macroscopic PEC analysis on the internal face of a spalled oxide (that is to say a part of the oxide scale which has been removed during spallation, size ~ 1 mm) was performed. This experiment, difficult to
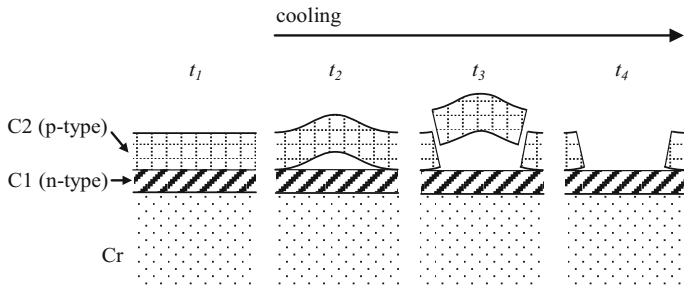
Fig. 6 First scenario via a classical process of buckling during the cooling of the sample. The separation of the scale occurs at the internal subscale/external subscale interface

implement, was possible using a small amount of silver paint in order to establish an ohmic contact on the back side of the sample (needed for the PEC experiment), i.e., the external face of the spalled oxide. In order to avoid any confusion for the reader, a schematic description of this experiment is presented in Fig. 7.

The macroscopic PEC result on the spalled oxide is presented in Fig. 8. The evolution of photocurrent and dephasing angle at low energy (< 3 eV) indicates, due to the use of silver paint, the presence of silver oxides, reported in the literature to exhibit a *n*- or *p*-type conduction with bandgaps of between 1.2 and 3.4 eV [41, 42].

At higher energy, only one contribution ($C1$) can be detected on the energy spectra (Fig. 8a) with a bandgap E_g around 3 eV. Again, the presence of only one contribution is confirmed with the stability near $-40°$ of the dephasing angle (Fig. 8b) in the whole range of energy higher than 3 eV. Figure 8c also confirms that $C1$ conduction remains mainly *n* (the photocurrent increases with the applied potential). This result is in contradiction with the previous hypothesis (*p*-type conduction was expected but *n*-type conduction is observed) and forces us to rethink a new scenario. We believe that during the cooling, the separation of the scale does not occur at the $C1/C2$ interface but at the metal/oxide interface. It is consequently
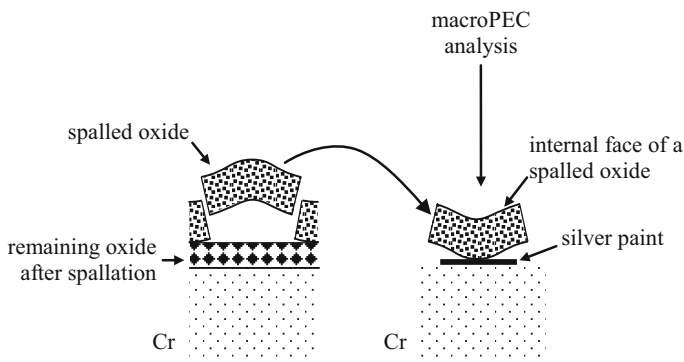

Fig. 7 Schematic presentation of the macroscopic PEC analysis performed on the internal face of a spalled oxide
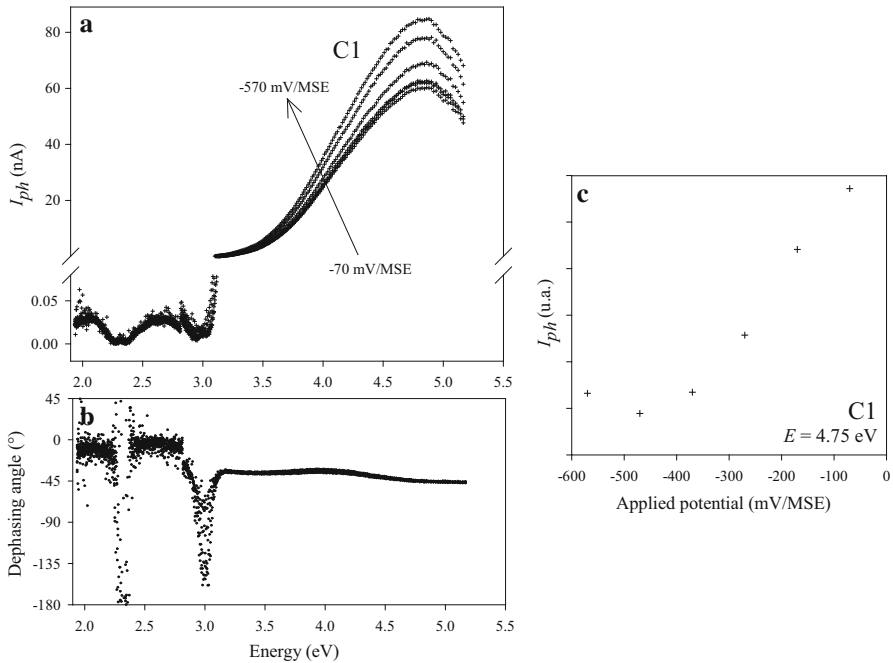
Fig. 8 PEC analysis on the internal face of a spalled oxide: **a** photocurrent (I_{ph}) and **b** dephasing angle versus incident light energy (E) recorded at several applied potentials (V) varying from − 570 to − 70 mV/MSE, with a 100 mV step, **c** photocurrent versus applied potential (V) at 4.75 eV from − 570 to − 70 mV/MSE, with a 100 mV step

assumed in this second scenario (presented in Fig. 9) that the metal/oxide interface is the most fragile, proposal consistent with the presence of microvoids observed by STEM at the beginning of "Results and Discussion" section. After separation, a regrowth of *n*-type chromia can occur. The regrowth of single *n*-type chromia (and not again a duplex structure *n* and *p*) can be explained if one assumes that the regrowth occurs during cooling. Indeed, at lower temperature (< 800 °C), thermodynamic calculations show that the nickel/bunsenite buffer generates an
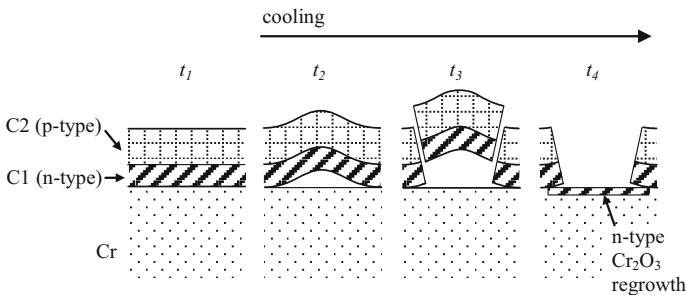
Fig. 9 Second scenario of buckling during the cooling of the sample. The separation of the scale occurs at the metal/oxide interface

oxygen partial pressure $p(O_2) < 10^{-14}$ atm. In these conditions, a previous work [16] has shown that only *n*-type chromia can be observed. To confirm this scenario, PEC measurements presented in Fig. 10 have been taken on a chromia scale grown at 800 °C and a $p(O_2) \sim 10^{-14}$ atm during 30 min. The energy spectra (Fig. 10a) reveal the expected single *C*1 contribution (bandgap $E_g \sim 3$ eV) confirmed with the stability near − 30° of the dephasing angle (Fig. 10b). Figure 10c again confirms that *C*1 conduction remains mainly *n* (the photocurrent increases with the applied potential).

The second scenario presented in Fig. 9 appears attractive, but a weak point must be underlined. Indeed, if the separation of the scale had really occurred at the metal/oxide interface, the spalled oxide studied by macroPEC in Fig. 8 should have been exhibited both *C*1 and *C*2 contributions, but only *C*1 was detected. We consider that during the preparation of the macroPEC experiment, the external part of the spalled oxide was possibly removed or, due to another undetermined reason, the *C*2 contribution could be not detected by the mesoPEC in this particular configuration. This second scenario also needs to be compared with others works. For example in 2003, Michalik et al. [43] have studied the role of water vapor in chromia scale growth on pure chromium at low oxygen partial pressure. The oxide scale formed at
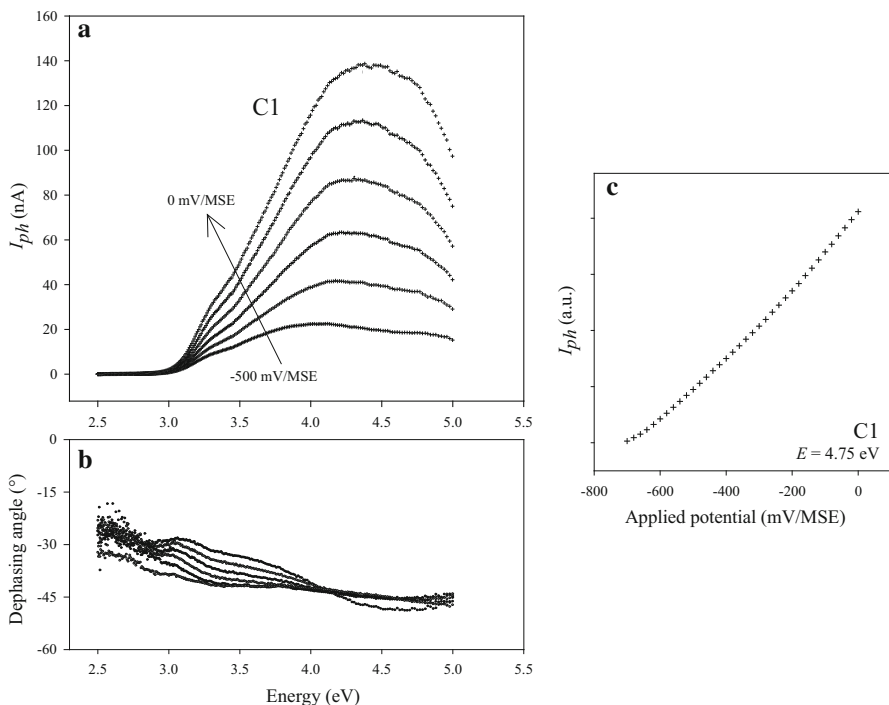
Fig. 10 PEC analysis PEC analysis performed chromia scale grown at 800 °C and a $p(O_2) \sim 10^{-14}$ atm during 30 min: **a** photocurrent (I_{ph}) and **b** dephasing angle versus incident light energy (E) recorded at several applied potentials (V) varying from − 500 to 0 mV/MSE, with a 100 mV step, **c** photocurrent versus applied potential (V) at 4.75 eV from − 500 to 0 mV/MSE, with a 100 mV step

high $p(O_2)$ exhibits a large number of pores and cracks parallel to the metal/oxide interface including long cracks in the oxide scale itself. By contrast, the scale morphology obtained at low $p(O_2)$ is totally different. The oxide scale appears to be very dense and adherent to the metal. However, oxide scale thicknesses are largely higher compared to the present study and low $p(O_2)$ are generated from Ar, H_2 and H_2O mixtures. In this case, it is not possible to separate the effect of the oxygen partial pressure and the effect of water vapor, well known to improve the adherence of oxide scales.

As an intermediate conclusion, the second scenario is consistent with the experimental observations obtained in this work but probably need to be consolidated with additional analysis. In particular, a STEM cross-sectional view close to the border of the spalled zone would be very useful to confirm the present hypothesis of a *n*-type chromia regrowth. However, this experiment is very complex to implement due to the debonded zone all around the spalled zone. As a consequence, the real interface between the spalled zone and the non-spalled zone is really difficult to identify (see the discussion at the beginning of "Results and Discussion" section). The effect of surface preparation is also probably very important. In the present work, samples were SiC ground up to the grade 320. More mesoPEC experiments with different surface preparations of the metallic chromium substrate should also bring interesting results.

Conclusions

Spallation observed on duplex chromia scales isothermally grown on pure chromium at 900 °C and a $p(O_2)$ of 10^{-12} atm during 30 min occurs during sample cooling. The separation of the scale takes place at the metal/oxide interface. The uncovered metal can be then reoxidized at lower temperature during the cooling. Photoelectrochemical techniques at a mesoscale (probe diameter in the range of 50 μm) have proven to be very successful in bringing innovative information thanks to the semiconducting signature of each subscale and in building a plausible spallation scenario.

References

1. P. Kofstad, *Oxidation of Metals* **44**, (1/2), 1995 (3–27).
2. W. C. Hagel and A. U. Seybolt, *Journal of the Electrochemical Society* **108**, (12), 1961 (1146–1152).
3. P. Kofstad and K. P. Lillerud, *Oxidation of Metals* **17**, (3/4), 1982 (177–194).
4. P. Kofstad and K. P. Lillerud, *Oxidation of Metals* **17**, (3/4), 1982 (195–203).
5. A. Holt and P. Kofstad, *Solid State Ionics* **69**, 1994 (127–136).
6. A. Holt and P. Kofstad, *Solid State Ionics* **69**, 1994 (137–143).
7. K. P. Lillerud and P. Kofstad, *Journal of the Electrochemical Society* **127**, (11), 1980 (2397–2409).

8. A. Atkinson, *Solid State Ionics* **12**, 1984 (309–320).
9. A. Atkinson and R. I. Taylor, in *Transport on Nonstoichiometric Compounds*, eds. G. Simkovich and G. Stubican, Vol. 285, NATO ASI Series B129 (Plenum Press, New York, 1984).
10. K. Hoshino and N. L. Peterson, *Journal of the American Ceramic Society* **66**, (11), 1983 (C202–C203).
11. A. C. S. Sabioni, B. Lesage, A. M. Huntz, J. C. Pivin and C. Monty, *Philosophical Magazine A* **66**, (3), 1992 (333–350).
12. A. C. S. Sabioni, B. Lesage, A. M. Huntz, J. C. Pivin and C. Monty, *Philosophical Magazine A* **66**, (3), 1992 (351–360).
13. P. Kofstad, in *High Temperature Corrosion* (Elsevier Applied Science, London/New York, 1988), pp. 114–120.
14. D. J. Young, in *High Temperature Oxidation and Corrosion of Metals* (Elsevier Applied Science, London/New York, 2008), pp. 119–122.
15. K. Arnold, G. Tatlock, C. Kenel, A. Colella and P. Matteazzi, *Materials at High Temperatures* **5**, 2017 (1–10).
16. L. Latu-Romain, Y. Parsa, S. Mathieu, M. Vilasi and Y. Wouters, *Corrosion Science* **126**, 2017 (238–246).
17. X. Ledoux, S. Mathieu, M. Vilasi, Y. Wouters, P. Del Gallo and M. Wagner, *Oxidation of Metals* **80**, (1–2), 2013 (25–35).
18. L. Latu-Romain, Y. Parsa, S. Mathieu, M. Vilasi, M. Ollivier, A. Galerie and Y. Wouters, *Oxidation of Metals* **86**, 2016 (497–509).
19. L. Latu-Romain, S. Mathieu, M. Vilasi, G. Renou, S. Coindeau, A. Galerie and Y. Wouters, *Oxidation of Metals* **88**, 2016 (481–493).
20. L. Latu-Romain, Y. Madi, S. Mathieu, F. Robaut, J.-P. Petit and Y. Wouters, *Corrosion Science* **101**, 2015 (193–200).
21. F. N. Rhines, *Transactions of the Metallurgical Society of AIME* **137**, 1940 (246–286).
22. Y. Madi, L. Latu-Romain, S. Mathieu, V. Parry, J.-P. Petit, M. Vilasi and Y. Wouters, *Corrosion Science* **87**, 2014 (218–223).
23. A. Loucif, J.-P. Petit and Y. Wouters, *Journal of Nuclear Materials* **443**, 2013 (222–229).
24. N. Pilling and R. Bedworth, *Journal of the Institute of Metals* **29**, 1923 (529–582).
25. D. R. Clarke, *Current Opinion in Solid State and Materials Science* **6**, 2002 (237–244).
26. J. J. Barnes, J. G. Goedjen and D. A. Shores, *Oxidation of Metals* **32**, (5/6), 1989 (449–469).
27. A. M. Huntz, *Materials Science and Engineering: A* **201**, 1995 (211–228).
28. S. Daghigh, J. L. Lebrun and A. M. Huntz, *Materials Science Forum* **251–254**, 1997 (381–388).
29. A. M. Huntz, S. Daghigh, A. Piant and J. L. Lebrun, *Materials Science and Engineering: A* **248**, 1998 (44–55).
30. A. M. Huntz and M. Schütze, *Materials at High Temperatures* **12**, 1994 (169–174).
31. Y. Wang, W. W. Gerberich and D. A. Shores, *Journal of Materials Research* **12**, 1997 (697–705).
32. D. Delaunay, A. M. Huntz and P. Lacombe, *Corrosion Science* **20**, 1980 (1109–1117).
33. J. Robertson and M. I. Manning, *Materials Science and Technology* **6**, 1990 (81–87).
34. D. J. Baxter and K. Natesan, *Reviews on High Temperature Materials* **5**, 1983 (149–250).
35. H. E. Evans and M. P. Taylor, *Surface and Coatings Technology* **94–95**, 1997 (27–33).
36. A. Galerie, F. Toscan, M. Dupeux, J. Mougin, G. Lucazeau, C. Valot, A. M. Huntz and L. Antoni, *Materials Research* **7**, (1), 2004 (81–88).
37. M. Kemdehoundja, J. L. Grosseau-Poussard, J. F. Dinhut and B. Panicaud, *Journal of Applied Physics* **102**, 2007 (093513).
38. A. Galerie, F. Toscan, E. N'Dah, K. Przybylski, Y. Wouters and M. Dupeux, *Materials Science Forum* **461–464**, 2004 (631–638).
39. R. Benaboud, P. Bouvier, J.-P. Petit, Y. Wouters and A. Galerie, *Journal of Nuclear Materials* **360**, 2007 (151–158).
40. A. S. Dorcheh, M. Schütze and M. C. Galetz, *Corrosion Science* **130**, 2018 (261–269).
41. J. F. Dierson and C. Rousselot, *Surface and Coatings Technology* **200**, (1–4), 2005 (276–279).
42. Y. C. Her, Y. C. Lan, W. C. Hsu and S. Y. Tsai, *Journal of Applied Physics* **96**, (3), 2004 (1283–1288).
43. M. Michalik, M. Hänsel, J. Zurek, L. Singheiser and W. J. Quadakkers, *Materials at High Temperatures* **22**, (3–4), 2005 (39–47).